May, 2002

Width-Wise Variation of Magnetic Tape Pack Stresses

Jonathan A. Wickert, *Carnegie Mellon University*
Y.M. Lee, *Carnegie Mellon University*

Width-Wise Variation of Magnetic Tape Pack Stresses

Y. M. Lee
Assoc. Mem. ASME

J. A. Wickert
Fellow ASME

Department of Mechanical Engineering,
Carnegie Mellon University,
Pittsburgh, PA 15213-3890

A model is developed for predicting the stress and displacement fields within a magnetic tape pack, where those quantities are allowed to vary in both the pack's radial and transverse (cross-tape) directions. As has been the case in previous analyses based upon one-dimensional wound roll models, the present approach accounts for the anisotropic and nonlinear constitutive properties of the layered tape, and the incremental manner in which the pack is wound. Further, such widthwise variation effects as differential hub compliance and nonuniform winding tension, which can be significant in data cartridge design, are also treated in the model. The pack is analyzed through a two-dimensional axisymmetric finite element model that couples individual representations of the hub/flange and layered tape substructures. The bulk radial elastic modulus of the tape, which depends on the in-pack radial stress, is measured for a variety of media samples, and a reduced-order model is developed to capture the nonlinear modulus-stress correlation. The stiffness matrix of the hub/flange at its interface with the media provides a mixed boundary condition to the tape substructure. In this manner, design-specific hubs can be readily analyzed, and criteria for their optimization explored. Simulations of several cartridge designs are presented, and the roles of hub compliance and wound-in tension gradient in setting the pack's stress field and cross-tape width change are discussed. [DOI: 10.1115/1.1460911]

1 Introduction

Magnetic data storage on flexible media has played an important role in computer systems since the early 1950s. Tape systems currently span a broad range of consumer and enterprise storage applications, including audio, video, instrumentation, and computer systems. Within the next decade, compact tape cartridges for computer data storage are projected to provide several terabytes of capacity through a nearly 50-fold growth in areal density and substantial reduction in media thickness. In the rapidly moving computer industry, tape storage systems remain competitive through their low storage cost per megabyte of data and their high capacity. The technologies of magnetic and optical disk recording, at least presently, do not offer the same combination of advantages, and while other emerging technologies do offer strengths in one or more areas, overall they do not meet the entire set of performance needs that tape cartridge drives address.

One application of magnetic tape systems is backup/restore missions on medium-to-large scale computers and networks. The number of cartridges required for such applications can grow to the hundreds or thousands for systems in the graphics, medical imaging, and entertainment industries. For instance, a large system with a thousand gigabytes of on-line disk capacity can require about 3000 to 5000 gigabytes to hold several full and daily incremental backups. Although a primary use of tape systems is for off-line and archival data storage, mass storage systems are today supplemented by automated robotic libraries that make tape storage a nearly on-line computer peripheral. With growth in network-based business and information retrieval systems, the accessibility and reliability of vast data libraries on magnetic tape remains an important technical issue.

As tape technology continues to migrate towards thinner media substrates (~4–5 μm), lower winding tensions (~0.28–0.56 N) and higher speeds (~7–10 m/s) to increase capacity and reduce access time, tape mechanics problems, for which solutions had been engineered, often recur. For instance, reductions of tape thickness and data track width provide the direct means to increase volumetric storage density, and therefore the capacity of a given sized cartridge. On the other hand, as the media becomes thinner, its handling and mechanical stability become more problematic. Over roughly the past decade, media substrates have been reduced in thickness from some 30 μm to 5 μm, and as track widths fall to several microns, the dimensional stability of the media in the presence of aggressive in-pack stresses likewise becomes critical. Uneven or excessive compressive stress within a cartridge can cause tape layers, individually or together, to buckle in the pack's radial direction, axial direction, or both. The photograph of Fig. 1 depicts a so-called spoking defect in which the tape layers buckled locally to such an extent that an internal gap formed. Such buckling is facilitated by the combined conditions of low radial stress, and high compressive circumferential or transverse stresses.

Traditionally, research on the stress field in magnetic tape packs or other types of wound rolls has emphasized one dimensional models wherein the hub and tape are each treated as being infinitely wide, and with uniform mechanical properties and tension across the width. Based on the constitutive properties specified for the media, the one-dimensional models can be categorized broadly into four groups: linearly elastic ([1–3]), linearly viscoelastic ([4–6]), nonlinearly elastic ([7–11]), and nonlinearly viscoelastic ([12]). Such studies consider only radial and circumferential stresses, treat the media as being orthotropic, specify that the hub has uniform cross-tape compliance, and ignore effects associated axial and shear stress components ([13]).

The tape pack itself is generally modeled as a layered structure which is developed incrementally as a succession of pretensioned hoops that are shrunk-fit onto the underlying pack. That process is a nonlinear one to the extent that the effective radial elastic modulus of the tape region, at the bulk level, is a function of the interlayer radial stress which in turn changes as the pack is formed. In short, the mechanical properties of a wound tape pack are often quite different from those of a single isolated layer because of entrained air and surface asperity contact. Accordingly, the bulk radial modulus plays an important role in pack stress modeling

Contributed by the Applied Mechanics Division of THE AMERICAN SOCIETY OF MECHANICAL ENGINEERS for publication in the ASME JOURNAL OF APPLIED MECHANICS. Manuscript received by the ASME Applied Mechanics Division, Mar. 1, 2001; final revision, Nov. 22, 2001. Associate Editor: R. C. Benson. Discussion on the paper should be addressed to the Editor, Prof. Lewis T. Wheeler, Department of Mechanical Engineering, University of Houston, Houston, TX 77204-4792, and will be accepted until four months after final publication of the paper itself in the ASME JOURNAL OF APPLIED MECHANICS.

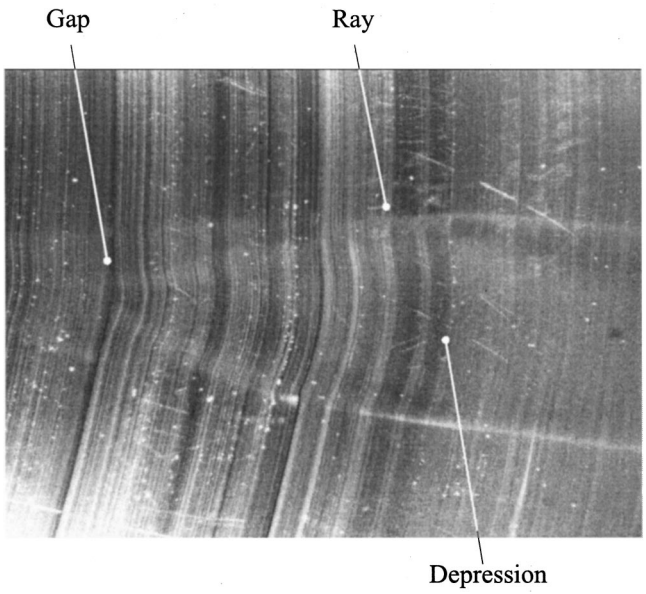

Fig. 1 Magnified view of a region in a magnetic tape pack exhibiting interlayer buckling

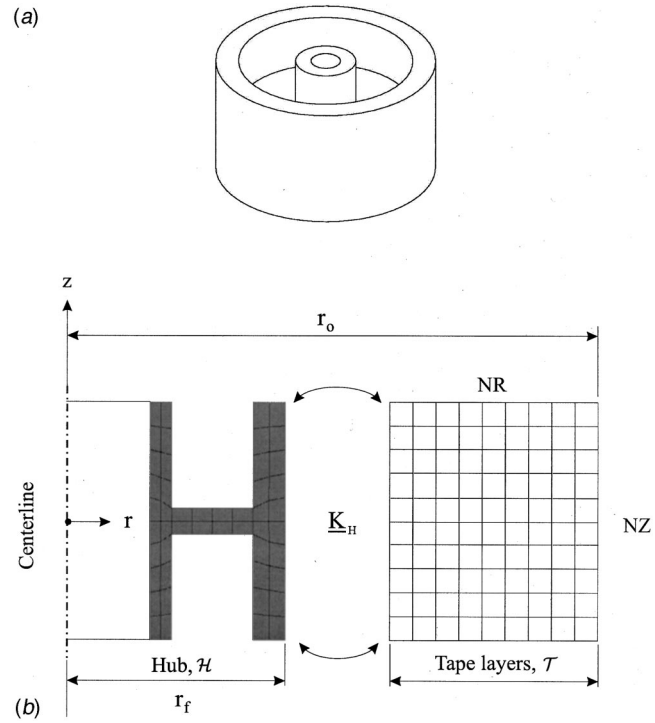

Fig. 2 (*a*) An axisymmetric hub that is also symmetric with respect to the pack's midplane, and (*b*) model of the hub and tape layer substructures

([8,9,14]). Since the media's substrate is typically a polymer such as PET (polyethylene terephthalate) or PEN (polyethylene naphthalate), viscoelastic effects, although not considered here, set the manner in which wound-in stresses relax over time. Other effects including wound-on tension losses, temperature, humidity, and finite deformation have also been studied in various applications ([3,10,11]).

Certain two-dimensional stress models have been considered with a view towards understanding stress dependencies which arise due to thickness variations across the width ([15–17]). The nonuniform widthwise winding tension was simulated by stacking web layers having varying widthwise thickness. Each of these approaches was based on the assumptions that the pack could be partitioned across its width into a discrete number of segments that do not couple, and that the stresses and displacements so developed are width-independent. Notably, shear-extension and bending-extension coupling were ignored in those treatments.

In what follows, a two-dimensional axisymmetric finite element model is developed in order to analyze the magnetic tape pack stress problem. The internal stresses are allowed to vary both in the pack's radial and axial directions, and four stress components—radial, circumferential, axial, and shear—as well as two displacements—radial and axial—are determined. The present approach is appropriate for treating realistic cartridge hub designs, nonuniform widthwise tension profiles which can result from guiding imperfections, and the tape's cross-track width change. Experiments are further discussed in which the bulk compressive radial modulus is measured for several media specimens. A reduced-order treatment of individual layer and nonlinear interface compression is discussed in order to model the experimental data and incorporate it into the stress analysis.

2 Finite Width Tape Pack Model

A magnetic tape pack is formed by winding a continuous stream of media, having specified tension and speed, onto a hub. In general, the hub will have a radial stiffness that varies across its width, and the hub's geometry and materials are designed and chosen to meet various functionality requirements. Shown illustratively in Fig. 2(*a*) is the so-called 9840-style cartridge hub which has a plane of symmetry with respect to the media's centerline. The central rib at the hub's centerline reinforces the structure and allows more tape to be wound at higher tension. Since the flanges and the hub connect only through a press-fit snap lock, the stiffness afforded to the hub by the flanges is neglected in this case. Figure 3(*a*) depicts a second type of hub design, termed 3480-style, which is a common format in the tape storage industry and which has no particular midplane symmetry. The cartridge's two flanges are formed from different materials, and the structure's cross-sectional geometry is generally step-shaped in order to facilitate attaching the hub to the drive motor's spindle.

By way of motivation, Fig. 4 indicates how the collocated point radial compliance of these two hub designs changes across the media's width. The ratio of the maximum-to-minimum compliance values for the symmetric hub design is roughly 5:1, and the ratio is roughly 4:1 for the asymmetric design. The cross-tape compliance variation is significant in each case, and sets the boundary condition afforded to the layered tape region at its interface with the hub. In what follows, the effects of differential hub compliance are explicitly treated in the pack stress model in order to develop a stress simulation of greater fidelity than is available through existing conventional one-dimensional models.

In Figs. 2 and 3, the tape has thickness h, and it is wound layer by layer into a nearly cylindrical shape having outer radius r_o and inner radius r_f common with the hub's winding face surface. Formed from N individual layers which are conceptually shrunk-fit onto one another in an incremental quasi-static manner, the tape region is treated as being a composite material having bulk anisotropic and nonlinear material properties. In general, the hub is an integral solid structure, and it is often made of fiber-reinforced plastic. In short, the material properties of the hub and tape regions can be substantially different.

In order for the analysis to properly account for various hub geometries, the tape pack is conceptually separated into the hub and tape substructures following the approach developed in [13]. The respective subdomains are denoted $\mathcal{H}=\{(r,\theta,z):r<r_f,0<\theta<2\pi,-w/2<z<w/2\}$ over the hub, and $\mathcal{T}=\{(r,\theta,z):r_f<r<r_o,0<\theta<2\pi,-w/2<z<w/2\}$ over the tape. For the symmetric hub shown in Fig. 2, the hub's winding face and outer radius are the same. For the asymmetric hub of Fig. 3, the winding face is

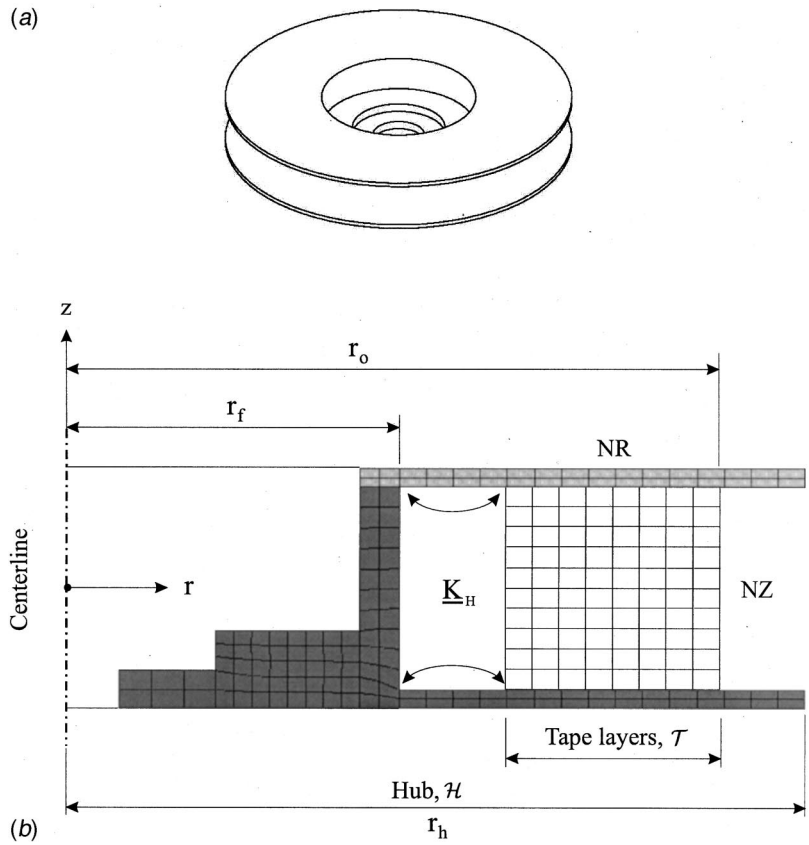

Fig. 3 (*a*) **An axisymmetric hub having no particular midplane symmetry, and** (*b*) **model of the hub and tape layer substructures**

located at a different radius than the hub's outer radius r_h owing to presence of the flanges. The substructures couple through the interfacial hub stiffness matrix $\mathbf{K}_H$ which affords a mixed boundary condition to the tape substructure. In order to effectively deal with the potential variety of hub materials and geometry, the hub itself is analyzed through a commercial finite element package, and $\mathbf{K}_H$ is extracted by sequentially applying unit loads along the hub-tape interface, and inverting the flexibility matrix so obtained.

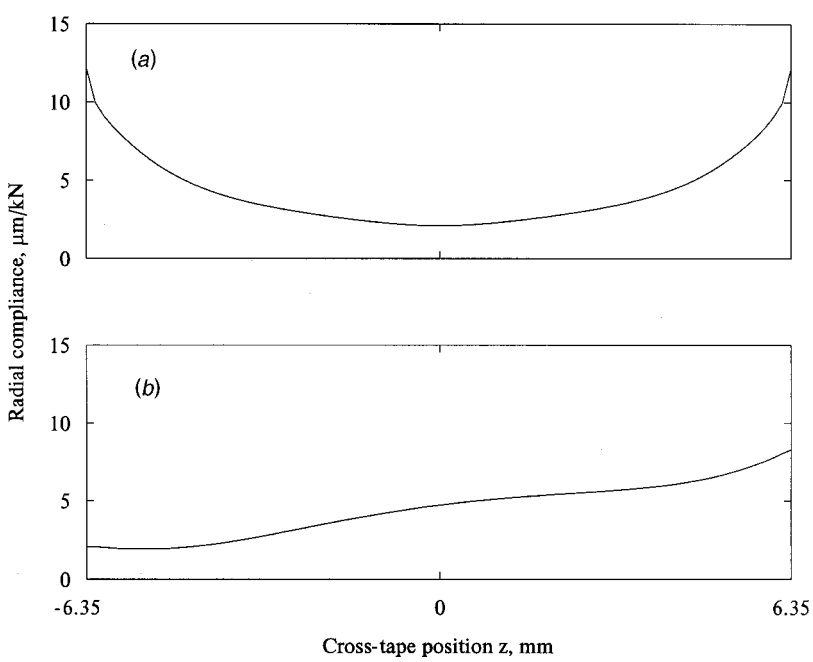

Fig. 4 Collocated point radial compliance of (*a*) **the symmetric hub of Fig. 2, and** (*b*) **the asymmetric hub of Fig. 3**

The stress field and displacements in $\mathcal{T}$ develop as each layer, a pre-tensioned cylindrical shell, is fit to the underlying pack. As the nth layer is added, for instance, the cumulative stresses $\boldsymbol{\sigma}_n$ within the pack are expressed $\boldsymbol{\sigma}_{n-1}+\Delta\boldsymbol{\sigma}_n$, where $\boldsymbol{\sigma}_{n-1}$ is the stress developed upon winding the first through $(n-1)$st layers, and $\Delta\boldsymbol{\sigma}_n$ is the incremental stress associated with addition of the final nth layer.

As the nth layer is added, $\mathcal{T}$ is discretized with bilinear axisymmetric elements. The governing equations comprise equilibrium, constitutive, and compatibility conditions, and they are functions of nodal displacements $\mathbf{a}=\{\mathbf{uw}\}^T$, where $\mathbf{u}(r,z)$ and $\mathbf{w}(r,z)$ are the radial and transverse components. The stiffness matrix in $\mathcal{T}$ is $\mathbf{K}_T=\Sigma_{i=1}^{NE}\mathbf{k}_i^e$, where $\mathbf{k}_i^e$ is the stiffness matrix for each element i, and NE is the number of elements in $\mathcal{T}$'s representation. The 8×8 elemental stiffness matrix becomes

$$\mathbf{k}_i^e=2\pi\int_{\mathcal{A}^e}\mathbf{B}_i^T\mathbf{E}_i\mathbf{B}_i dA^e, \tag{1}$$

where A^e is the element's $r-z$ cross-sectional area, $\mathbf{B}_i$ is the derivative of the strain-displacement relation, and $\mathbf{E}_i$ is the material's elasticity matrix. In turn, the structure-level stiffness matrix of the entire pack becomes $\mathbf{K}_P=\mathbf{K}_H+\mathbf{K}_T$, where proper assembly of the matrices accounting for the interfacial nodes at $r=r_h$ is implied. In addition, the nodal loads for the entire pack are evaluated as $\mathbf{F}=\Sigma_{i=1}^{NE}\mathbf{f}_i^e$ where the elemental nodal load is given by

$$\mathbf{f}_i^e=2\pi\int_{\delta A^e}\mathbf{N}_i^T\mathbf{t}_i r d\delta A^e+2\pi\int_{A^e}\mathbf{B}_i^T\mathbf{D}_i\boldsymbol{\epsilon}_{0i}d\mathcal{A}^e-2\pi\int_{A^e}\mathbf{B}_i^T\boldsymbol{\sigma}_{0i}d\mathcal{A}^e. \tag{2}$$

Here $\mathbf{N}_i$ is the bilinear shape function, and $\boldsymbol{\epsilon}_{0i}$ and $\boldsymbol{\sigma}_{0i}$ are the initial strain and stress for each element. The governing equations become $\mathbf{K}_P(\mathbf{a})\mathbf{a}=\mathbf{F}$ and are written in terms of the nodal displacements $\mathbf{a}$.

Solutions are subject to specified displacement and traction boundary conditions. For instance, the boundary conditions for a cartridge with the symmetric hub of Fig. 2 include vanishing transverse displacement at $(r_i,0)$ in order to suppress the rigid body motion. The general traction boundary conditions include

- vanishing traction at all hub surfaces excluding the positions with specified displacement boundary conditions,
- $\sigma_z=\sigma_{rz}=0$ over the upper and lower tape surfaces $z=\pm w/2$ and $r\in[r_f,r_o]$,
- $\sigma_{rz}=0$ and $\sigma_r=T(z)/(w(r_f+(n-1)h))$ over the outer tape surface $r=r_o$ and $z\in[-w/2,w/2]$

where r_i and w are the hub's inner radius and the tape's width, and the winding tension $T(z)$ is specified.

As the media's bulk radial modulus is known to depend strongly on stress, as each layer or group of layers is added to an existing pack, a truncated Taylor expansion is used to linearize the governing equations about either an initial estimate or a converged result obtained from calculation at the preceding state. Computation through Newton-Raphson iteration begins by evaluating $\mathbf{K}_P$ at an initial estimate $\mathbf{a}^*$. In the first iteration, the nodal displacements become $\mathbf{a}_1=\mathbf{K}_P^{-1}(\mathbf{a}^*)\mathbf{F}$. The vector of imbalanced nodal loads in the second iteration becomes $\Delta\mathbf{f}_2=\mathbf{F}-\mathbf{K}_P(\mathbf{a}_1)\mathbf{a}_1$. The incremental nodal displacements $\Delta\mathbf{a}$ in the second iteration are $\Delta\mathbf{a}_2=\mathbf{K}_P^{-1}(\mathbf{a}_1)\Delta\mathbf{f}_2$, and the cumulative displacements at that stage become $\mathbf{a}_2=\mathbf{a}_1+\Delta\mathbf{a}_2$. Iteration proceeds until the solution satisfies a specified convergence criterion expressed in terms of the norm $\eta^2=\Sigma\Delta a_j^2/\Sigma a_j^2$. When η falls below a specified tolerance, say 10^{-3} as in the case studies below, the solutions are said to have converged relatively, and iteration is terminated. With the nodal displacements so obtained, the stresses over element i are incremented by $\Delta\boldsymbol{\sigma}_{ni}=\mathbf{D}_i(\mathbf{B}_i\mathbf{a}_i-\boldsymbol{\epsilon}_{0i})+\boldsymbol{\sigma}_{0i}$, and the cumulative stresses advance to $\boldsymbol{\sigma}_{(n-1)}+\Delta\boldsymbol{\sigma}_n$.

Table 1 Baseline parameter values used in the pack winding case studies

Property	Hub Symmetric	Asymmetric
Modulus, E	2.5 GPa	3.5 GPa
Poisson ratio, ν	0.43	0.43
Outer radius, r_f	11.43 mm	25.00 mm
	Tape	
Tension, T_0		1.0 N
Number of layers, NL		3000 —
Width, w		12.7 mm
Thickness, h		10.0 μm
Bulk radial modulus, E_r		$7000/(1+10.7\sigma_r^{-0.77})$ MPa
Circumferential modulus, E_θ		7 GPa
Transverse modulus, E_z		9 GPa
Shear modulus, G_{rz}		100 MPa
Poisson ratio, $\nu_{\theta z}=\nu_{\theta r}=\nu_{zr}$		0.3 —

3 Media Bulk Radial Modulus

Region $\mathcal{T}$ is well approximated as being orthotropic and axisymmetric, and so some four elastic moduli (E_r, E_θ, E_z, and G_{rz}) and six Poisson ratios ($\nu_{r\theta}$, ν_{rz}, $\nu_{\theta z}$, $\nu_{\theta r}$, ν_{zr}, and $\nu_{z\theta}$) must be specified to complete the formulation. The values for these material properties, exclusive of E_r, are developed following the discussion presented in reference [13], and they are listed in Table 1.

The media's substrate, magnetic and tribological coatings, and interfaces each contribute to E_r. The radial modulus was measured through compression tests conducted with a conventional materials testing machine. Each stack of experimental media had dimensions 102 mm×12.7 mm×12.7 mm. When such samples are extracted from an existing pack or larger format pancake, it is possible for irregular or distorted edges to be present, and such effects are minimized by having the compression plates be smaller in diameter than the samples' lengths. A 5 kN load cell was used to measure the applied force, and an extensometer with gage length 25.4 mm and 20 percent extension to measure the displacement across the sample. During manufacturing, a wide web of magnetic media is slit into many individual streams of tape, which in turn are wound on large format hubs so as to store the media temporarily prior to forming data cartridges. The diameters of such pancakes typically vary from 200–300 mm, and the samples used in these studies were cut from such pancakes.

For a particular experimental media, Fig. 5 illustrates a representative stress-strain response over five successive tests. The behavior during the first load cycle differs somewhat from the subsequent ones as most of the air entrapped between adjacent layers is expelled during that first load-unload cycle. The experimental data are fit to a polynomial through least squares regression, and the bulk modulus is determined by differentiating the stress-strain expression. Figure 6 depicts measured response of the specimen over a full load-unload cycle, and the behavior is clearly path-dependent. The area enclosed by the loading and unloading curves represents the energy dissipated during the process as caused by the internal material damping and interfacial friction, among other factors. Such path-dependent behavior can be used to simulate the full winding and unwinding process.

In order to examine potential variability in E_r for media samples extracted from a single pancake, and namely from the same tape stream and widthwise position on the manufacturing web, samples were removed from the pancake from three different radii, each at a different circumferential location. Because the pancake is substantially larger than a typical data cartridge and the stress field within it varies substantially with position, each sample was presumably produced and stored under a different stress history. It is an objective here to assess variability in E_r associated with the production process, quite aside from the wound roll model itself. Measured moduli for the nine media

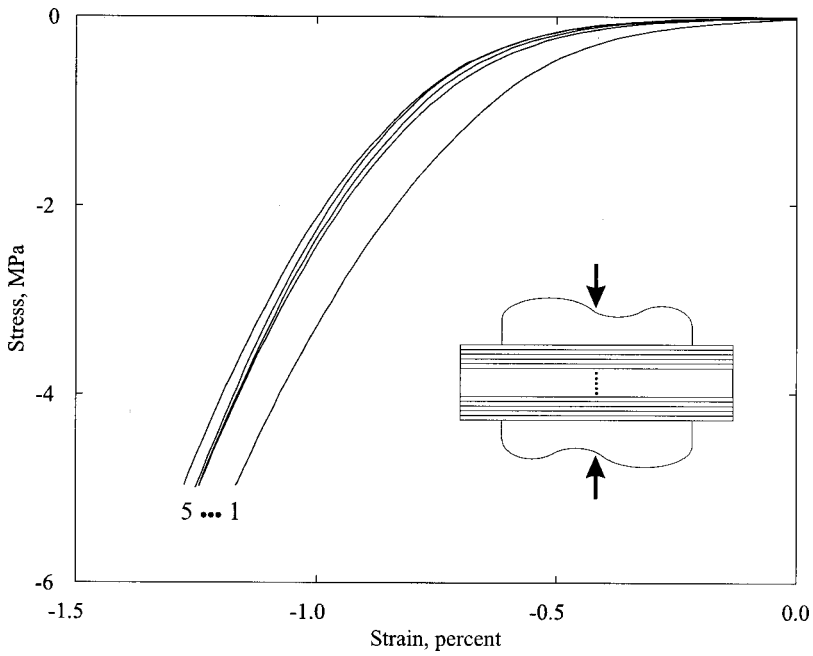

Fig. 5 Measured stress-strain response in compression of a magnetic tape stack over five loading cycles; sample dimensions: 102 mm×12.7 mm×12.7 mm

samples are shown in Fig. 7(*a*), where some variability among the samples depending on radial location within the pancake is evident. At a fixed value of stress, say 2 MPa, E_r varies between roughly 800 and 1200 MPa, or ± 20 percent about its mean value. The three samples taken from the outer periphery of the pancake consistently exhibited lower E_r than those extracted from the inner periphery, consistent with the notion of the media undergoing slight strain hardening as asperities are plastically deformed during the pancake's formation.

In considering a media stack under uniform compression, its bulk deformation arises both from compression of the substrate layers and compliance of the surfaces. Considering N layers, there are $N-1$ interfaces formed by adjacent contact of the magnetic surface on one layer, and the backcoat surface on another. Both the tape layers and the interfaces contribute to the macroscopic stiffness, and this assemblage is modeled accordingly as a series of elastic springs. Specifying that the substrate deforms linearly during compression, the elastic constant contributed by the tape's

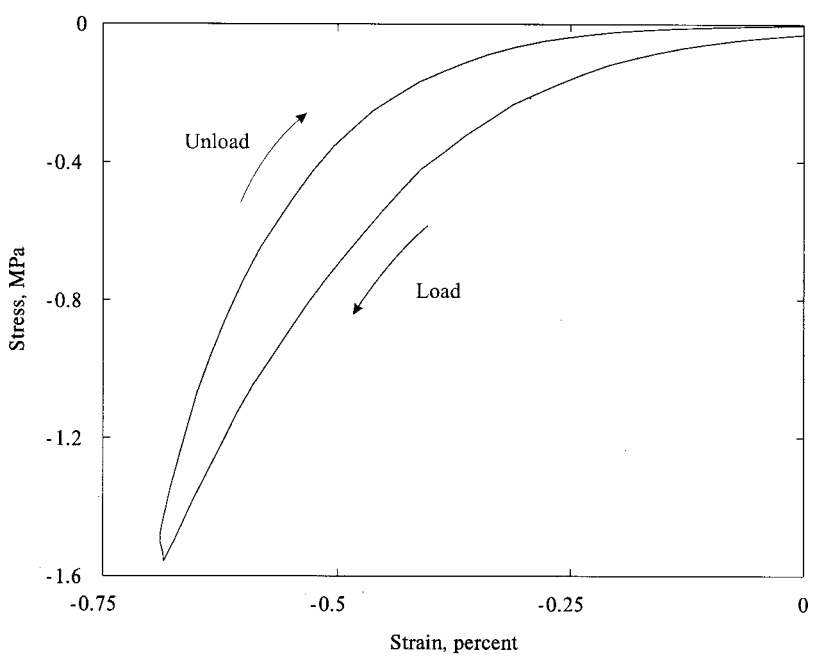

Fig. 6 Typical measured stress-strain response of a magnetic tape stack over a single load–unload cycle; sample dimensions: 102 mm×12.7 mm×12.7 mm

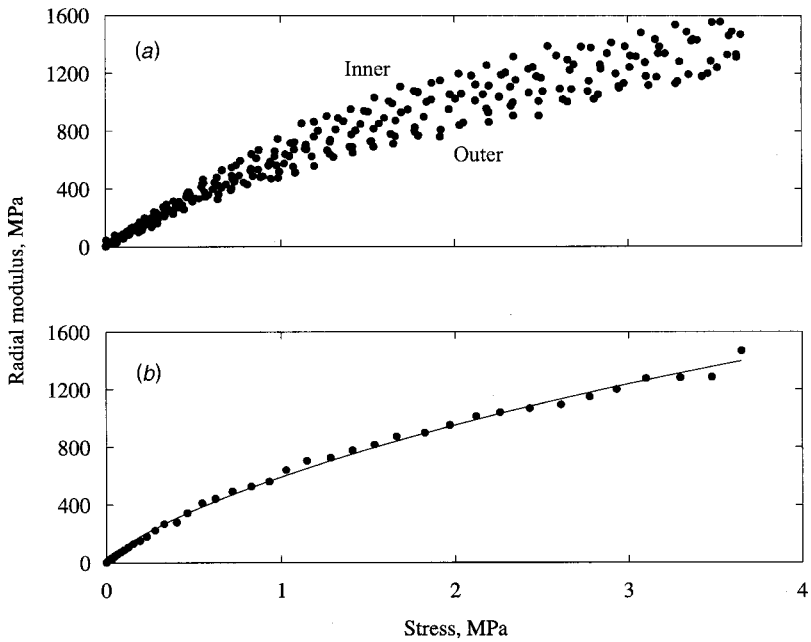

Fig. 7 (*a*) Variability of the measured bulk radial modulus for nine nominally identical media samples. (*b*) Measurements averaged over all samples (● ● ● ●), and the least-squares fit to the modulus model (——); $c=1.61\times10^{7}$ N/mm$^{4.26}$ and $m=3.26$.

substrate for each layer is $k_s=EA/h$, where E and A are the elastic modulus and apparent contact area for a single layer. The real area of contact, in turn, increases with the compressive load ([18]). The interfacial stiffness changes in response to its deformation with constant $k_i=(c\Delta_i)^m$, where c and m are constants determined subsequently through a fit to the data. For pure Hertzian contact of similar materials, for instance, $c=16E^2\beta/9$ and $m=1/2$, where β is the radius of an individual asperity's summit. Extension to rough but nominally flat surfaces in contact is discussed by [18].

Under compressive load P, the stack's total deformation becomes $\Delta=N\Delta_s+(N-1)\Delta_i\approx N(\Delta_s+\Delta_i)\approx N(P/k_s+P/k_i)$ for large N. By definition, the strain in the media's stack is $\epsilon=\Delta/(Nh)=(P/k_s+P/k_i)/h=P/(E_rA)$. Following algebraic manipulation, the bulk radial modulus is expressed

$$E_r=E\left(1+\frac{EA}{h}\frac{1}{\sqrt[m+1]{c^mP^m}}\right)^{-1} \tag{3}$$

as a function of applied stress. The unknown parameters c and m are determined by fitting the experimental data through a least square method. Figure 7(*b*) demonstrates the manner in which Eq. (3) captures the measured data.

4 Stress Field With Symmetric Hub Design

Figures 8 and 9 depict the predicted radial and circumferential stress distributions as functions of r and z for the hub design of Fig. 2 and parameter values as given in Table 1. Pack formation was simulated with a winding tension of 1 N having uniform stress 7.87 MPa over the tape's cross section. In Fig. 8, σ_r increases from zero at the pack's outer periphery to reach its maximum compressive value of -2.45 MPa along the hub-tape interface at the location $(r,z)=(11.43,0)$ mm of the hub's central reinforcement rib. The radial stress is less compressive near the tape's edges where the hub has greater compliance. For the first layer on the hub, σ_r varies from -1.48 MPa at the tape's edges to -2.45 MPa at the centerline, an increase of some 70 percent. Such cross-width variation of in-pack stresses is significant in Figs. 8–9 over only about one-third of the pack, as indicated by the contour diagrams shown as insets in the figures. With respect to the circumferential stress, the maximum value occurs at r_f on the tape's edges at the position $(11.43,\pm6.35)$ mm. Further, σ_θ varies from -7.73 MPa at the edges to -1.21 MPa at the centerline for the pack's first layer. Notably, σ_θ is compressive at the pack's innermost radial positions, grows to become tensile in the outer layers, and precisely equals the winding stress at the outermost layer. The bold demarcation line in the contour diagram inset in Fig. 9 indicates the loci of points where $\sigma_\theta=0$, in order to aid in understanding the locations of such pack buckling defects as seen in Fig. 1. In this simulation, the transverse σ_z and shear σ_{rz} stresses are significant only near the hub-tape interface and arise from the strain mismatch between the different materials forming $\mathcal{H}$ and $\mathcal{T}$. Since the edges of the pack model are traction free and coupling ν_{rz} between the r and z directions is almost zero, σ_z and σ_{rz} are likewise negligible away from r_f.

4.1 Cross-Track Media Width Change. The in-pack stresses in turn cause the tape's width to change slightly, and as the pack would be subsequently unwound, those dimensional changes would be reflected as variations in the spacing of data tracks. Figure 10 shows the predicted tape width change Δw as a function of position along the tape's length based on the stress fields of Figs. 8–9. To the extent that the viscoelastic relaxation time of the media is long when compared to the time required for the pack to unwind, Δw would be measured and compensated by the read-write head's servo system. The width change is calculated by subtracting the tape's transverse displacements at the upper and lower edges, and the difference increases gradually from the outer periphery with a rapid increase near $\mathcal{H}$. The maximum value reached in this case study is about 14 μm or 1100 ppm, which is in fact greater than the roughly 5 μm data track width on a modern drive. As shown in Fig. 10, more than 35 percent of the pack is subjected to a width change greater than a single track width.

4.2 Cross-Tape Tension Gradient. Figures 11 and 12 illustrate the radial and circumferential stress fields as functions of r and z for a pack wound under tension that varies linearly across

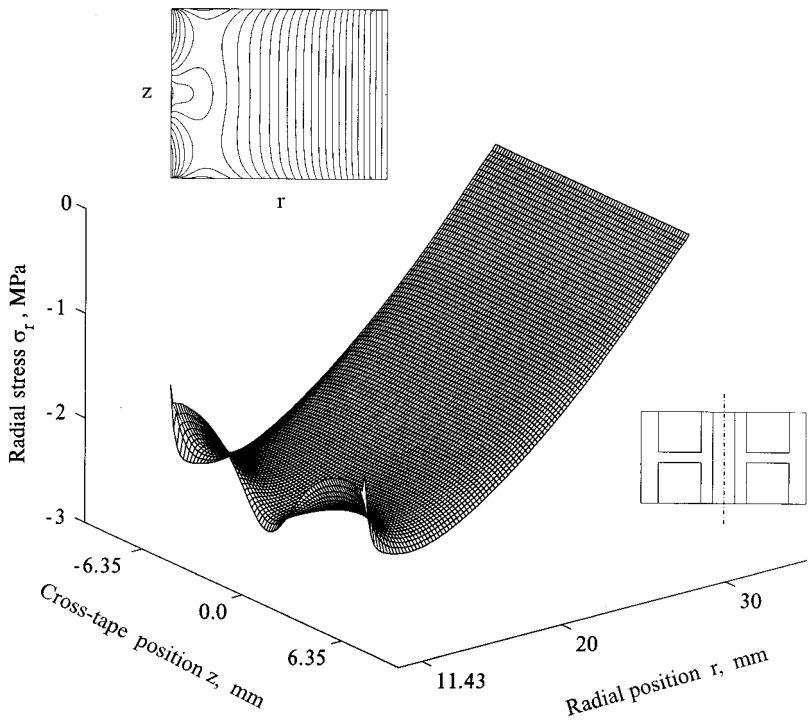

Fig. 8 Radial stress field in the symmetric hub case study. The insets depict the hub's cross section and a contour representation of σ_r over the $r-z$ plane; constant tension, $NR=100$, $NZ=80$.

the tape's width. Such a situation arises when the tape bends in the transport path either as a result of guide misalignment or tape lateral motion. The tension profile is approximated by a quadratic function as $T(z)=c_2z^2+c_1z+c_0$, where c_2, c_1, and c_0 are set by specified values at the tape's edges and centerline.

In Figs. 11 and 12, the tension is specified to vary from $0.75\,T_0$ at the bottom edge $z=-6.35$ mm to $1.25\,T_0$ at the top edge $z=6.35$, where T_0 is the nominal tension. The resulting tension profile becomes $T(z)=(z/2w+1)T_0$ over $z=[-w/2,w/2]$. Cross-tape variations of σ_r and σ_θ are more prominent in Figs. 11

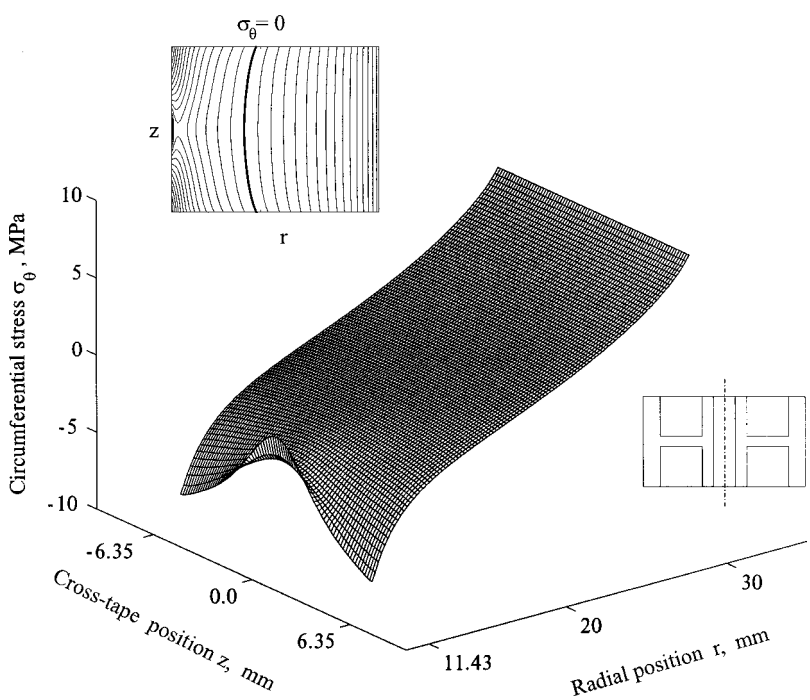

Fig. 9 Circumferential stress field in the symmetric hub case study. The insets depict the hub's cross section and a contour representation of σ_θ in the $r-z$ plane; constant tension, $NR=100$, $NZ=80$

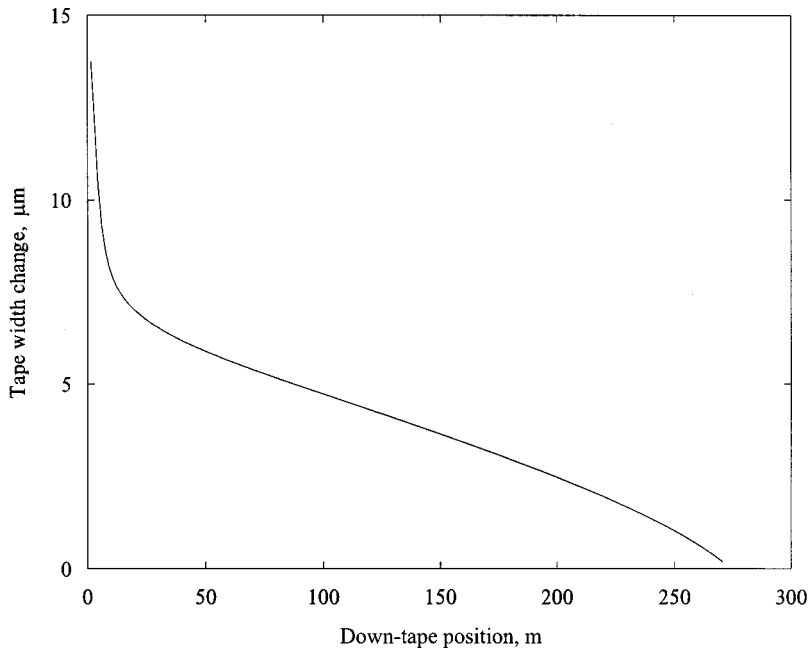

Fig. 10 Predicted change in tape width. The maximum value at the hub-tape interface is about 14 μm, or 1100 ppm.

and 12 than for the case of a uniform tension profile in Figs 8 and 9. Along the tape's higher tension edge, both the radial and circumferential stresses in Figs. 11 and 12 have higher magnitudes. As was the case in Figs. 8 and 9, the maximal compressive radial stress occurs at the location of the central reinforcement rib is located. With respect to the extreme values of σ_r at the first layer, the ratio of the maximum and minimum values is 2.4:1, somewhat larger than 1.7:1 as in the uniform tension case study. Component σ_θ has a more uneven distribution, and the ratio of the extreme values here is 9.4:1, with the maximum compressive value of -11.1 MPa occurring at (11.43,6.35) mm.

In some circumstances, the winding tension is known to roll-off at both edges of the tape in a manner well approximated as $T(z)=(-(z/w)^2+1)T_0$. The radial and circumferential stresses

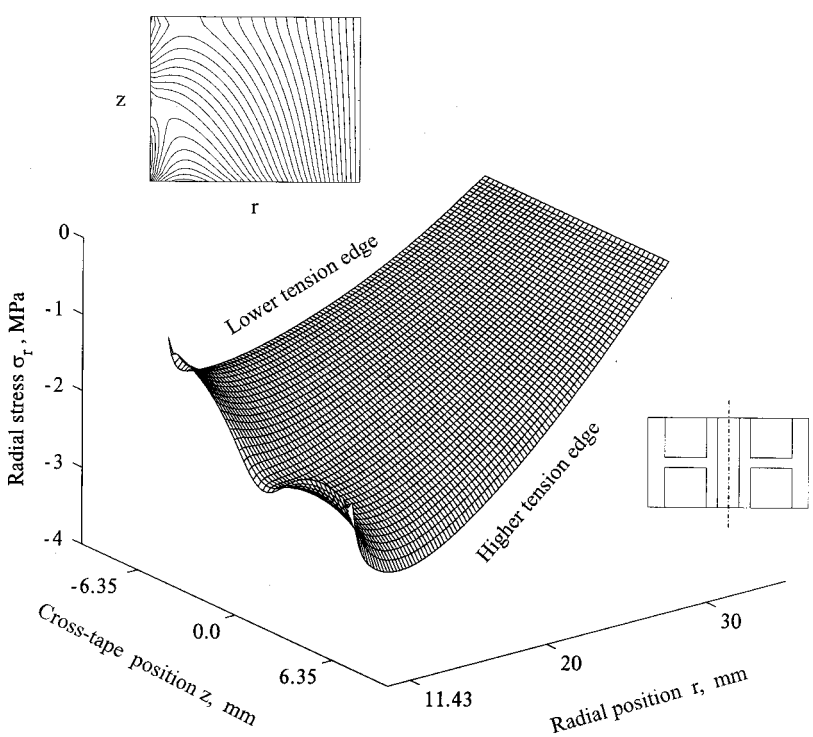

Fig. 11 Radial stress field in the symmetric hub case study. The insets depict the hub's cross section and a contour representation of σ_r in the $r-z$ plane; linear cross-tape tension gradient, $NR=100$, $NZ=80$.

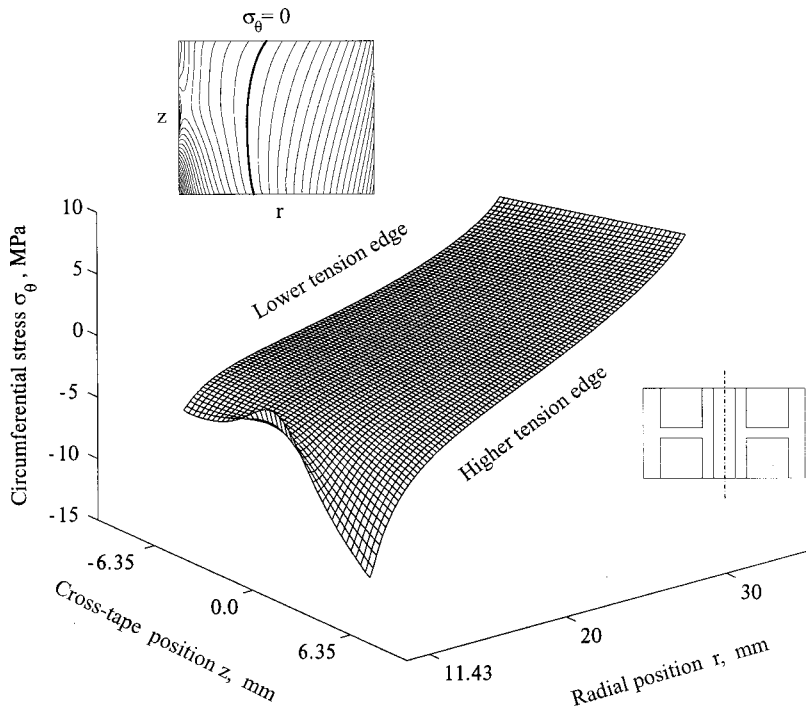

Fig. 12 Circumferential stress field in the symmetric hub case study. The insets depict the hub's cross section and a contour representation of σ_θ in the $r-z$ plane; linear cross-tape tension gradient, $NR=100$, $NZ=80$.

resulting from this tension profile are shown in Figs. 13 and 14. Here σ_r and σ_θ are less compressive than in the case of uniform tension, but they do vary to a greater extent across the tape's width. Here the ratios of the extreme values at the first layer for σ_r and σ_θ are 2.2:1 and 6.2:1, respectively.

5 Stress Field With Asymmetric Hub Design

In the case of the asymmetric hub format of Fig. 3, the in-pack stress field is expected to be singular at the intersecting corners of the hub's winding face and the flanges, to the extent that those

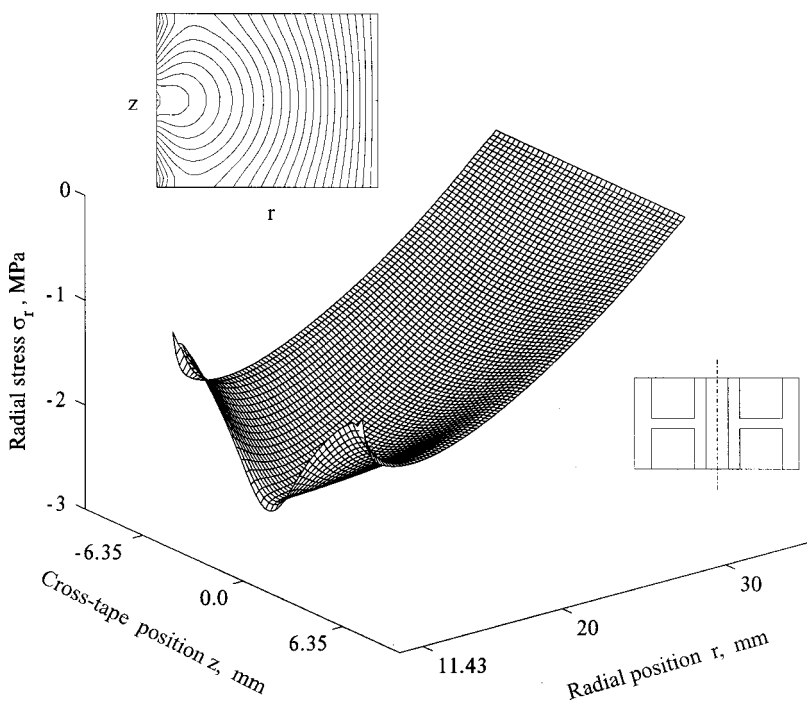

Fig. 13 Radial stress field in the symmetric hub case study. The insets depict the hub's cross section and a contour representation of σ_r in the $r-z$ plane; parabolic cross-tape tension gradient, $NR=100$, $NZ=80$.

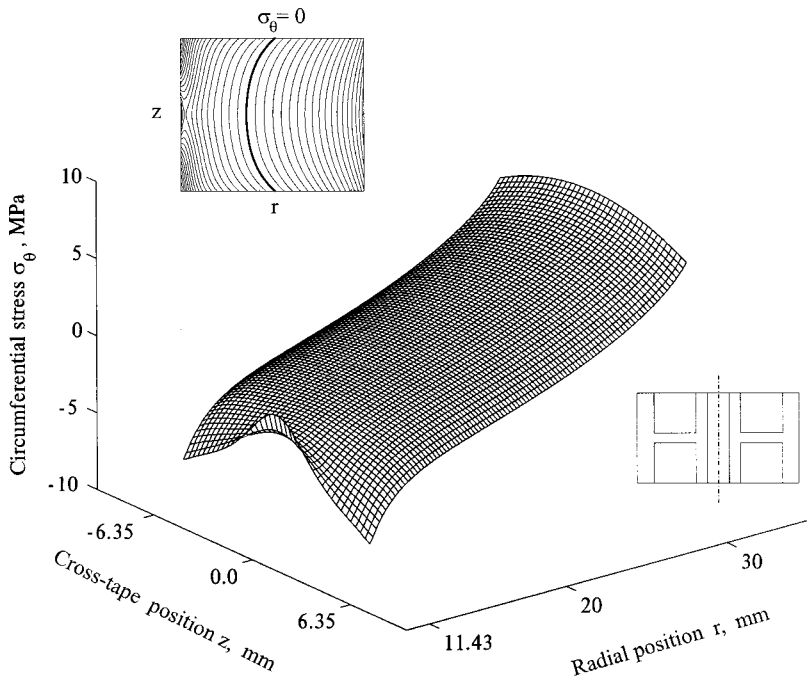

Fig. 14 Circumferential stress field in the symmetric hub case study. The insets depict the hub's cross section and a contour representation of σ_θ in the $r-z$ plane; parabolic cross-tape tension gradient, $NR=100$, $NZ=80$.

components are formed of dissimilar materials ([13,19]). Stress behavior at those regions was investigated through a mesh refinement convergence study. Figure 15(a) shows the predicted radial stresses along the pack's centerline and edges as functions of radial position for $NZ=40$ and 80. Stress σ_r converges well along the centerline and throughout most of the pack, except for the narrow regions near the hub-tape interface. Figure 15(*b*) shows the distribution of σ_r in the first layer as a function of cross-tape position. The radial stress converges over some 90 percent of the cross section at $NZ=80$ except for regions adjacent to the corners. The domain of convergence expands with increasing NZ as the singularity further localizes.

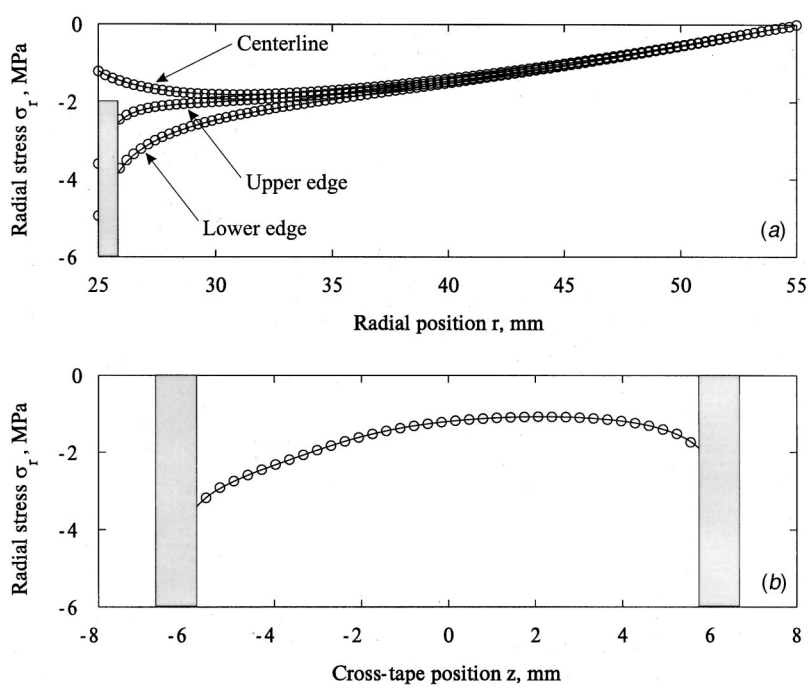

Fig. 15 Radial stress distribution (*a*) in the down-tape direction at three positions across the width, and (*b*) across the tape's width at the hub-tape interface; $NZ=40$ (○ ○ ○ ○) and $NZ=80$ (——). Shaded zones indicate where the solution did not converge to three significant figures.

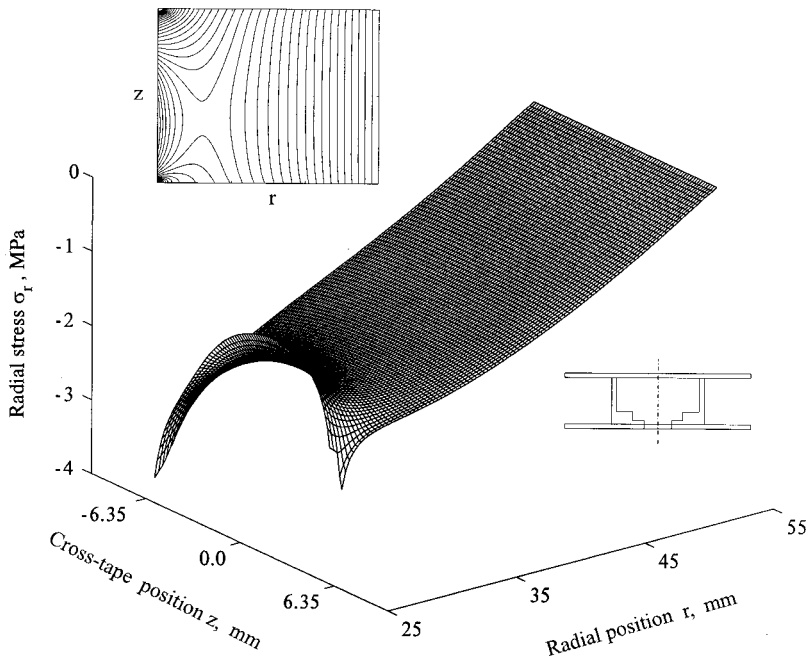

Fig. 16 Radial stress field in the asymmetric hub case study. The insets depict the hub's cross-section and a contour representation of σ_r in the $r-z$ plane; constant tension, $NR=100$, $NZ=80$.

Figures 16 and 17 show the radial and circumferential stresses as functions of r and z only in the domain over which the solution has fully converged. The singular behavior at the corners strongly affects σ_r over the first several layers of tape, and it exhibits a sudden increase in compression near the corners. Even though the upper portion of the hub is comparatively compliant, the high gradients dominate the σ_r distribution. Likewise, stress σ_θ varies significantly along the hub-tape interface from 2.30 MPa at the pack's bottom edge to -8.97 MPa at the top edge. The bold demarcation line in the inset contour diagram of Fig. 17 represents the loci of points where $\sigma_\theta=0$. It is interesting to note that the pack's bottom edge is not in circumferential compression, evidently suggesting that it is more stable from the defect formation perspective than regions near the top surface.

6 Summary

A finite width model for predicting the stresses and displacements within a magnetic tape cartridge has been discussed. Such widthwise variations as differential hub stiffness and nonuniform

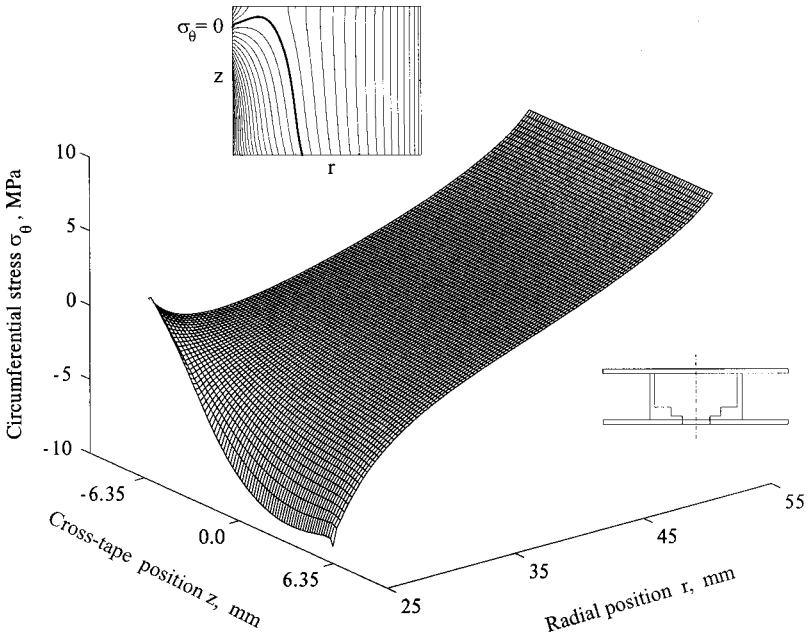

Fig. 17 Circumferential stress field in the asymmetric hub case study. The insets depict the hub's cross section and a contour representation of σ_θ in the $r-z$ plane; constant tension, $NR=100$, $NZ=80$.

winding tension are explicitly treated in the formulation. The solution is developed through finite element and substructuring methods in order to handle a potential variety of hub geometries and materials. The cross-tape tension gradient as is caused by guide misalignment, scatterwinding, and tension roll-off is also modeled with a view towards understanding the in-pack stress field as a precursor to defect formation.

Measurements of the media's bulk radial modulus were performed through compression tests and demonstrate that such values do depend on the specimen's stress history and location within the manufacturing pancake. The heuristic reduced-order model for E_r was shown to represent the measured data, and aside from polynomial curve fits as have been used previously, provides a meaningful bound with increasing σ_r. In case studies with two typical hub designs, the simulations quantify the roles of differential hub compliance, hub design, and winding tension gradients in setting the pack's internal stress distribution.

Acknowledgment

This work was supported in part by Imation Corporation through the Advanced Tape Systems Program, and by the National Science Foundation. The authors appreciate the assistance and comments of Durkee Richards, William Qualls, and Chris Merton of Imation Corporation, Bill Buchan of Seagate Technology, and Ted Schwarz of Peregrine Recording Technology.

References

[1] Altmann, H. C., 1968, "Formulas for Computing the Stresses in Center-Wound Rolls," Journal of the Technical Association of the Paper and Pulp Industry, **51**, pp. 176–179.

[2] Yagoda, H. P., 1980, "Resolution of a Core Problem in Wound Rolls," ASME J. Appl. Mech., **47**, pp. 847–854.

[3] Connolly, D., and Winarski, D. J., 1984, "Stress Analysis of Wound Magnetic Tape," ASLE Tribology and Mechanics of Magnetic Storage Media, Special Publication 16, ASLE, pp. 172–182.

[4] Tramposch, H., 1965, "Relaxation of Internal Forces in a Wound Reel of Magnetic Tape," ASME J. Appl. Mech., **32**, pp. 865–873.

[5] Tramposch, H., 1967, "Anisotropic Relaxation of Internal Forces in a Wound Reel of Magnetic Tape," ASME J. Appl. Mech., **34**, pp. 888–894.

[6] Heinrich, J. C., Connolly, D., and Bhushan, B., 1986, "Axisymmetric, Finite Element Analysis of Stress Relaxation in Wound Magnetic Tapes," ASLE Trans., **29**, pp. 75–84.

[7] Hakiel, Z., 1987, "Nonlinear Model for Wound Roll Stresses," Journal Tech. Assoc. Paper Pulp Indust., **70**, pp. 113–117.

[8] Willett, M. S., and Poesch, W. L., 1988, "Determining the Stress Distributions in Wound Reels of Magnetic Tape Using a Nonlinear Finite-Difference Approach," ASME J. Appl. Mech., **55**, pp. 365–371.

[9] Zabaras, N., Liu, S., Koppuzha, J., and Donaldson, E., 1994, "A Hypoelastic Model for Computing the Stresses in Center-Wound Rolls of Magnetic Tape," ASME J. Appl. Mech., **61**, pp. 290–295.

[10] Good, J. K., Pfeiffer, J. D., and Giachetto, R. M., 1992, "Losses in Wound-on Tension in the Centerwinding of Wound Rolls," *Web Handling*, ASME AMD-149, ASME, New York, pp. 1–12.

[11] Benson, R. C., 1995, "A Nonlinear Wound Roll Model Allowing for Large Deformation," ASME J. Appl. Mech., **62**, pp. 853–859.

[12] Qualls, W. R., and Good, J. K., 1997, "An Orthotropic Viscoelastic Winding Model Including a Nonlinear Radial Stiffness," ASME J. Appl. Mech., **64**, pp. 201–208.

[13] Lee, Y. M., and Wickert, J. A., 2002, "Stress Field in Finite Width Axisymmetric Wound Rolls," ASME J. Appl. Mech., submitted for publication.

[14] Bhushan, B., 1992, *Mechanics and Reliability of Flexible Magnetic Media*, Springer-Verlag, New York.

[15] Hakiel, Z., 1992, "On the Effect of Width Direction Thickness Variations in Wound Rolls," *Second International Conference on Web Handling*, Oklahoma State University, pp. 79–98.

[16] Kedl, D. M., 1992, "Using a Two Dimensional Winding Model to Predict Wound Roll Stresses that Occur due to Circumferential Steps in Core Diameter or to Cross-Web Caliper Variation," *Second International Conference on Web Handling*, Oklahoma State University, pp. 99–112.

[17] Cole, A., and Hakiel, Z., 1992, "A Nonlinear Wound Roll Stress Model Accounting for Widthwise Web Thickness Nonuniformities," *Web Handling*, ASME AMD-149, ASME, New York, pp. 13–24.

[18] Greenwood, J. A., and Williamson, J. B. P., 1966, "Contact of Nominally Flat Surfaces," Proc. R. Soc. London, Ser. A, **A295**, pp. 300–319.

[19] Bogy, D. B., 1970, "On the Problem of Edge-Bonded Elastic Quarter-Planes Loaded at the Boundary," Int. J. Solids Struct., **6**, pp. 1287–1313.